POLARIZATION OF GRB BY SCATTERING OFF RELATIVISTICALLY MOVING MATERIAL: COMPTON SAILING AND HIGH POLARIZATION

Amir Levinson[1,2] and David Eichler[3]
Draft version February 2, 2008

ABSTRACT

The polarization of gamma ray emission scattered off the baryon rich material that collimates a GRB fireball and the coasting speed of the irradiated matter are calculated numerically for different geometries of the radiation source and the collimating wall. It is shown that when the scattering material is Compton sailing, the direction of maximum polarization is quite generally well within the beaming cone of scattered radiation. As a result, the probability for observing bright highly polarized GRB's increases considerably, provided the Lorentz factor of the coasting matter is not well below 30, and the scattered radiation is highly polarized even when the beam thickness is large compared to $1/\Gamma$. It is suggested that correlation between polarization and intensity could provide clues as to whether energy flows from matter to photons or the reverse.

Subject headings: black hole physics — gamma-rays: bursts and theory

1. INTRODUCTION

Gamma ray bursts (GRB's) are believed to contain about 10^{51} ergs in the form of several $\times 10^{57}$ photons averaging several hundred KeV in energy. On the other hand, they are believed to have Lorentz factors of at least 10^2, and, hence, at most $\sim 10^{51}$ protons. For each proton, there must be at least 10^5 photons/baryon emitted. The question arises: what determines the number of photons emitted per baryon and why should the average photon energy in a GRB be consistently close to the electron rest mass?

A popular model posits that these photons are emitted as synchrotron radiation in an optically thin environment, typically at distances 10^{13} to 10^{15} cm. However, this begs the question of why a) the synchrotron frequency in the lab frame, which depends on the magnetic field, b) the comoving Lorentz factor γ' of the emitting electrons, c) the bulk Lorentz factor Γ, and d) the viewing angle together so frequently conspire to put the peak luminosity near 300 KeV. The fact that this peak energy has been observed to vary from ~ 2 MeV all the way down to ~ 10 KeV notwithstanding, we contend that the typical value of several hundred KeV is remarkable. For example, the strong linear correlation in the HETE II data set (Atteia et al. 2003) between the square root of the isotropic equivalent fluence E_{iso} and the spectral peak $h\nu_{peak}$, $h\nu_{peak}/100KeV \sim [E_{iso}/10^{52}\mathrm{erg}]^{1/2}$, suggests that the softer GRB's are intrinsically weaker and quite possibly merely the peripheries of GRB jets. The bright bursts show remarkably little variation in the location of the spectral peak.

A detailed analysis by Preece et al. (2002) shows that even if the spectral peak distribution could be arranged within the optically thin synchrotron model, the spectra at low energy, which typically show $dn_\gamma/dE \propto E^{-1}$, are inconsistent with optically thin, efficiently cooling synchrotron emission which would give $dn_\gamma/dE \propto E^{-3/2}$. (It could be argued that the bulk Lorentz factor Γ is fre-

quently high enough that the synchrotron cooling is inefficient, which would give a harder spectrum, but then it becomes hard to understand how the emission, which depends on a high power of Γ in this regime, is frequently so efficient.) The recent claim of high polarization in GRB's (Coburn and Boggs 2003) has nevertheless strengthened the views of some that the emission mechanism is optically thin synchrotron (e.g. Lyutikov, Parlev and Blandford 2003). Others have argued that the claimed degree of polarization, 70 to 80 percent (but with considerable experimental uncertainty), is too high to be accommodated by this mechanism, which limits the polarization to at most 56 percent for the case of a wide beam, $\Delta\theta \gg 1/\Gamma$.

At the time of this writing, the observational situation is, in the opinion of the authors, unresolved on several fronts. The significance of the X-ray flashes is not yet fully understood. The degree of polarization estimated by Coburn and Boggs may be considered uncertain by several factors: e.g. large error bars, the chance proximity of the modulation frequency of the RHESSI detector and the intrinsic variability of GRB021206, including 2s variability in the hardness (Hajdas et al. 2003), and the absence of other bursts to date that could establish how typical this burst was. Much of the motivation for the model discussed in this paper is thus tentative, but it should be clear that working out the predictions theoretically is part of the process of resolving the issues observationally.

An alternative model has been developed in a series of papers (Levinson and Eichler, 1993, 2000, 2003; Eichler and Levinson 1999, 2000, 2003; Eichler 1994, 2003; van Putten and Levinson 2002, 2003) originally and still motivated by the above questions. Its basic assumption is that the extreme baryon purity that must exist in the high Γ GRB outflows is enforced by the event horizon of a central black hole, so that the original baryonic content in the outflow must vanish. The photosphere near the axis of the outflow is therefore at about the annihilation radius of the pairs, which until then constitute the main component of

[1] School of Physics & Astronomy, Tel Aviv University, Tel Aviv 69978, Israel; Levinson@wise.tau.ac.il

[2] School of Physics, University of Sydney, NSW 2006

[3] Physics Department, Ben-Gurion University, Beer-Sheva 84105, Israel; eichler@bgumail.bgu.ac.il

the fireball plasma. The fireball's ability to manufacture more photons drops precipitously beyond the $e^{\pm}$ annihilation radius, so the total photon entropy of the GRB is frozen near its value at pair annihilation, when the average energy per photon is of the order of magnitude of $m_e c^2$. [Actually, the comoving temperature should be about an order of magnitude (the log of the compactness parameter) less than $m_e c^2$ if there is perfect thermal equilibrium, but the dissipation introduced by the friction of the fireball with the surrounding walls probably introduces some non-equilibrium signature on the spectrum, and the bulk Lorentz factor is probably at least a few even in the presence of such friction.]

In this class of models, the average photon energy in a GRB, though somewhat dependent upon the geometry of the walls and how the photons bounce off them, is naturally of order $m_e c^2$ without fine tuning of the parameters. As long as photons can bounce off the walls at large angles and make pairs with other outgoing photons, the dissipation continues, the expansion is accompanied by additional photon production, and the bulk Lorentz factor remains moderate. As soon as the energy density is below that needed to maintain pairs, transparency sets in and the photon entropy remains nearly constant thereafter.

Yet another class of models posits that GRB's are photons that are upscattered optical/UV photons by relativistic electrons with a Lorentz factor of order 300 (Shaviv and Dar 1995a, b; Lazzati et al. 2000; Dado, Dar, and De Rujula 2003). In these models, the number of photons is conserved and the energy of the outgoing photons, which is provided by the Compton scattering material, has been increased by a factor of 10^5 to 10^6. Thus, the once scattered photons constitute the primary GRB beam. Because the number of photons is conserved, the isotropic equivalent luminosity of the Compton scattered photons is of order Γ^4 times that in the optical/UV photons. If the latter is of order the Eddington luminosity for a $10 M_{\odot}$ star, then the observed isotropic luminosities for bright bursts, 10^{13} to $10^{15} L_{edd}$ require Lorentz factors exceeding 10^3. Shaviv and Dar (1995) predicted in their model that inverse Compton emission is expected to emerge polarized with a correlation between polarization and other quantities associated with the angle of observation. This should include overall fluence and peak luminosity, which are down from the peak values by factors of 8 and 16 respectively when the polarization is at a maximum. The high polarization is possible only when the angular width of the beam is narrower than $1/\Gamma$, and this constrains the solid angle of the beam to be extremely small if high net polarization is to be observed.

The Compton upscattering model for polarization (Dar and Shaviv 1995) should be compared and contrasted to the ensheathment model of Eichler and Levinson (1999). Both models predicted linear polarization before the announced discovery (Coburn and Boggs 2003) In the ensheathment model, the energy of the photon is not necessarily increased by the scattering and certainly not by a dramatic factor. The photons can thus originate in a much smaller region without violating the black body limit, and short timescales are, in principle, possible even for the once scattered radiation (the criticism of Lazzati et al. on this point is therefore not justified). The scattering

material in the ensheathment model may have a relatively moderate bulk Lorentz factor and the solid angle of the scattered light can subtend a much larger angle than the high Γ scattering material invoked by the Compton upscattering models. It is therefore possible to combine a large (lab frame) scattering angle and high polarization. It is also easy in the ensheathment model to have a geometry in which only scattered radiation is seen by the observer. As proposed by Eichler and Levinson (1999), the large reduction of the "on-axis" luminosity that was apparently achieved by GRB980425/SN1998bw, perhaps 4 or 5 orders of magnitude, comes with only modest reduction of frequency. It can result from a small fraction of photons being scattered, by a non-relativistic or modestly relativistic scatterer, into such a large angle as to be observable by us. The smooth light curve that was observed for GRB980425, rare among GRB's and far removed from the relation of Atteia et al. (2003), is consistent with the light having reached us via many different paths.

In recent years, the view that GRB's are collimated (e.g. Levinson and Eichler 1993)has been almost universally accepted, and the collimating matter is probably a host star or a wind. This confirms the assumption that GRB fireballs pass through some sort of surrounding wall in their early stages. This has particular significance for models in which the early fireball is baryon-free, because it provides a source of baryon seeding that could account for afterglow-generating plasma escaping intact to infinity. In the first place, some baryons are introduced downstream as entrained matter or pick-up neutrons that diffuse into the outflow from surrounding walls of baryonic matter. This matter can be a host star or simply a baryonic wind driven from the accretion disk of the black hole. The baryonic density in this picture has a complicated transverse structure (Levinson and Eichler 2003), the density increases outward, and the photosphere can be close to the pair annihilation radius near the axis, about 10^{10} cm, and near the walls at the edge (see Fig. 1).

In this paper, we consider another source of baryons - the collimating walls themselves - and note that, due to the impact of the GRB photons on the walls, relativistic motion of the walls can ensue. This matter can then be considered part of the GRB. It can cause highly polarized gamma ray emission in certain viewing directions and can cause afterglow. It might even be the case that there is a smooth transition from the supernova ejecta to the GRB fireball. This could account, for example, for the peculiar features of SN 1998bw, which has a huge expansion velocity (c/6) and peculiar abundances.

This was considered by Eichler (2003, hereafter E03) under simplifying geometric assumptions: that the photons emerged from a small, effective point source. It was argued that the photon pressure would accelerate the wall material to a Lorentz factor of $1/sin\chi$, where χ is the angle between the photon flow and the wall, and that the polarization of scattered photons off the wall would be greater than 0.6 with considerable probability. Here we relax the point source assumption. In section 2 we consider the terminal Lorentz factor in the presence of a photon field from a finite source, whose shape is characterized by two parameters. In section 3, we consider the effect of finite source size on the expected polarization. Finally, we con-

sider multiple scattering within a localized neighborhood of the point of photon impact on the sheath.

We demonstrate that in the present model, large polarization (of order 40 percent) is typical even when the beam "acausal", i.e. when it has a much larger opening angle than $1/\Gamma$. This is not the case in most models where the intensity along the line of sight typically receives contributions from a surrounding neighborhood of velocity vectors within the beam, whereby the polarizations of the various contributing beams cancel. In the limit of axisymmetric contribution around the line of sight, this cancellation would be complete. In the present model, on the other hand, there is a lower degree of symmetry (hence the calculations are unfortunately more complicated), because the incident radiation arrives from a direction much different (even in the comoving frame) from the velocity vector.

2. POLARIZATION BY A COMPTON SAILING SHEATH

We consider the dynamics of the inner layers of the baryon rich sheath surrounding the baryon poor core, and the consequent polarization of the scattered gamma-ray emission. We envision that the sheath is irradiated by the gamma-ray source which is located at small radii, as illustrated in Fig 1. The radiative force would accelerate the inner layers, leading to a strong shear of the boundary layer. Viscous forces may counteract the radiative force, and the profile of the Lorentz factor across the boundary layer would, in general, depend on the detail of momentum transfer between the moving layers of the sheath. In the limit of a highly super-Eddington primary photon luminosity, it seems likely that the radiation pressure overwhelms the viscous forces on the exposed layers of scattering material. This case has been considered in E03, and is explored further below.

2.1. Dynamics

The stress-energy tensor of a magnetized flow is given by

$$T^{\alpha\beta} = hnU^\alpha U^\beta - p\eta^{\alpha\beta} + \frac{1}{4\pi}(F^{\alpha\sigma}F^\beta_\sigma + \frac{1}{4}\eta^{\alpha\beta}F^2), \quad (1)$$

where $F_{\mu\nu}$ is the electromagnetic tensor, $U^\alpha = (\Gamma, \Gamma\vec{\beta})$ is the 4-velocity of the bulk fluid, and n, p, and h, are the proper particle density, pressure and specific enthalpy, respectively. The energy, momentum and continuity equations can be written as

$$\partial_\alpha T^{\alpha\mu} = S^\mu,$$
$$\partial_\alpha(nU^\alpha) = 0. \quad (2)$$

The above set of equations must be augmented by Maxwell equations for the electromagnetic field. The source term S^μ accounts for all external forces acting on the MHD flow, and is expressed here as the sum of a radiative force and all other forces (e.g., viscosity mediated by some instabilities, electromagnetic stresses, or diffusing neutrons; see Levinson and Eichler 2003): $S^\mu = S^\mu_c + S^\mu_2$. In terms of the distribution functions of gamma rays, f_γ, and electrons (we don't distinguish here between electrons and positrons), f_e, the source term associated with the radiative force is given, in the limit of Thomson scattering, by (see e.g., Phinney 1982),

$$S^\mu_c = -c\sigma_T \int \frac{d^3p_e}{u^0} \int \frac{d^3p_\gamma}{p^0_\gamma} f_\gamma f_e u_\alpha p^\alpha_\gamma [p^\mu_\gamma + (u_\nu p^\nu_\gamma)u^\mu], \quad (3)$$

where p^μ_e and p^μ_γ are the 4 momenta of electrons and gamma rays, respectively, as measured in the Lab frame, and $u^\mu = p^\mu_e/m_e$ is the corresponding electron 4 velocity. The gamma-ray distribution function satisfies a Boltzman equation:

$$p^\mu_\gamma \partial_\mu f_\gamma(p_\gamma, x) = C_\gamma(f_\gamma, p_\gamma, x), \quad (4)$$

where the collision operator must satisfy, $\int p^\mu_\gamma C_\gamma d^3 p_\gamma = -S^\mu_c$, by virtue of energy and momentum conservation. Once S^μ_2 is specified, the above set of equations, subject to appropriate boundary conditions, can, in principle, be solved to yield the structure and dynamics of the boundary layer. A complete treatment will be presented elsewhere.

In what follows, we consider, for illustration, the case of a sufficiently cold fluid dominated by radiative forces. By sufficiently cold we mean that to a good approximation the electron distribution function is given by $f_e = \Gamma n_e \delta^3(p^i_e - m_e U^i)$, where n_e is the electron proper density. We further suppose that the system is stationary and axially symmetric. Projecting eq. (2) on the direction perpendicular to the wall, defined by the unit vector $\hat{n}_s$, and using eq. (1), yields the pressure gradient required to support the corresponding component of the radiative force:

$$\hat{n}_s \cdot \vec{\nabla}(p + B^2/8\pi) = -\frac{\sigma_T n_e \Gamma}{c} \int d\nu \int d\Omega I_\nu (1 - \beta\mu) \sin\theta. \quad (5)$$

Here, $I_\nu = p^3_\gamma hcf_\gamma$ is the gamma ray intensity, and $\mu = \cos\theta$ denotes the cosine of the angle between the direction of impinging photons and the fluid velocity. The zeroth component of eqs. (2) yields

$$\vec{\beta} \cdot \vec{\nabla}(h\Gamma + B^2/4\pi n) = -\frac{n_e \sigma_T}{nc} \times$$
$$\int d\nu \int d\Omega I_\nu(\Omega)(1 - \beta\mu) \left[\Gamma^2(1 - \beta\mu) - 1\right], \quad (6)$$

where the continuity equation has been used.

The intensity at a given point on the wall generally receives contribution from both direct illumination of the radiation source and from reflection from other parts of the sheath that are exposed to the radiation source. To calculate the intensity we must therefore solve a transfer equation that accounts for multiple scattering between the different parts of the wall, as well as for diffusion of photons outward into the denser parts of the sheath. Since the reflected emission is beamed due to the relativistic motion of the sheath, it is clear that eq. (6) and the transfer equation obeyed by the intensity are coupled. The solution of the radiative transfer equation is beyond the scope of this paper. To simplify the analysis, we consider, in what follows, direct irradiation of the wall by an effective radiation source of a finite extent. From eq. (6) it is evident that for sufficiently large incidence angles of the impinging photons, the fluid will quickly accelerates to its coasting speed at which the component of the radiative force in the direction of motion nearly vanishes (E03).

In order to calculate the Lorentz factor of the coasting layer, we suppose that the incident radiation is emitted

4

from a surface defined by $S = S(x, y, z)$. The coordinate system adopted is shown in Fig. 1. The z axis is chosen to coincide with the symmetry axis. We denote by $\vec{r}_\beta$ the position vector of a fluid element, and by $\vec{r}_\gamma$ the position vector of a point on the gamma-ray emitting surface. The direction of an incident photon emitted from a point defined by $\vec{r}_\gamma$ is then given by (see Fig. 1)

$$\hat{k}_i = \frac{\vec{r}_\beta - \vec{r}_\gamma}{|\vec{r}_\gamma - \vec{r}_\beta|}. \tag{7}$$

The geometry of the radiation source adopted in the calculations presented below is shown in Fig. 2. The gamma-ray emitting surface has a geometry of a ring with inner and outer radii denoted by a_1 and a_2, respectively. The ring lies in the (x, y) plane at $z = 0$. The radius of the wall at $z = 0$ is denoted by d, and is normalized such that $d = 1$. The baryonic wall is taken to be conical for convenience. We note, however, that the difference between a conical wall and a curved one (as in the case of collimation) is only in the definition of d. In the latter case d represents the radius of a fictitious cone that extends from the location of the scattering material along the velocity vectors. The intensity in the source is taken to be homogeneous, that is, independent of x and y inside the ring (and zero outside, of course). The spectrum of incident radiation is taken to be a power law with index $\alpha = 0.5$ ($I_{in} \propto \nu^{-\alpha}$). The ring emission is allowed to be beamed. The beaming is parametrized by an angle θ_γ, measured with respect to the symmetry (z) axis. For a given beaming angle θ_γ, only rays that satisfy the condition $\hat{k}_i \cdot \hat{z} = \cos(\theta_\gamma)$ for the $\hat{k}_i$ given by eq. (7) can scatter off a fluid element located at $\vec{r}_\beta$.

In the coasting regime the R.H.S of eq. (6) nearly vanishes, and the solution of eq. (6) reduces to

$$\beta = \kappa - (\kappa^2 - 1)^{1/2}, \tag{8}$$

with

$$\kappa = \frac{\int d\nu \int d\Omega_s I_\nu (1 + \mu^2)}{2 \int d\nu \int d\Omega_s \mu I_\nu}, \tag{9}$$

where the inner integration is carried over the gamma-ray emitting surface, S, with $d\Omega_s = (d\hat{S} \cdot \vec{r}_\beta / r_\beta^3)$.

In the limit $a_1 = a_2 = 0$ that corresponds to a point source located on the symmetry axis, the intensity is given by $I \propto \delta(\mu - \mu_0)$, with $\mu_0 = z/(z^2 + d^2)^{1/2}$, and eq. (8) reduces to $\beta = \mu_0$, recovering the result obtained by E03.

2.2. Polarization

Consider now the polarization of the radiation scattered by the moving wall. Using the coordinate system depicted in Fig.1, we express the velocity vector of a fluid element, measured with respect to the Lab frame, as $\vec{\beta} = \beta(\sin\theta_\beta \cos\phi_\beta \hat{x} + \sin\theta_\beta \sin\phi_\beta \hat{y} + \cos\theta_\beta \hat{z})$, and the line of sight direction as $\hat{n} = \sin\theta_n \cos\phi_n \hat{x} + \sin\theta_n \sin\phi_n \hat{y} + \cos\theta_n \hat{z}$. The vector $\hat{k}_i$ given by eq. (7), and the vector $\hat{n}$ are transformed into the comoving frame of the fluid element (henceforth denoted by prime), using the aberration formula: $\cos\theta'_{i\beta} \equiv \hat{k}'_i \cdot \hat{\beta} = (\hat{k}_i \cdot \hat{\beta} - \beta)/[1 - \beta(\hat{k}_i \cdot \hat{\beta})]$, and likewise for $\cos\theta'_{n\beta} = \hat{n}' \cdot \hat{\beta}$.

Let $I_{in}(\vec{r}_\gamma, \hat{k}_i, \nu)$, with $\hat{k}_i$ given by eq. (7), denote the intensity of the incident radiation. In the rest frame of the fluid element it is given by $I'_{in}(\vec{r}_\gamma, \hat{k}'_i, \nu') = \delta_i^3 I_{in}(\vec{r}_\gamma, \hat{k}_i, \nu)$, where $\delta_i = \nu'/\nu = [\Gamma(1 + \beta\cos\theta'_{i\beta})]^{-1}$ is the corresponding Doppler factor. The polarization vector in the comoving frame lies along the direction $\hat{t} = \hat{n}' \times \hat{k}'_i / |\hat{n}' \times \hat{k}'_i|$. In terms of the unit vector $\hat{e} = \hat{n}' \times \hat{\beta}/|\hat{n}' \times \hat{\beta}|$, the Stokes angle is $\cos\chi = \hat{t} \cdot \hat{e}$. The comoving emissivity is given by

$$j'_\beta = \frac{3}{16\pi}\sigma_T n'_e \int I'_{in}(1 + \cos\psi'^2)d\Omega_s, \tag{10}$$

and the corresponding Stokes parameters by

$$\begin{pmatrix} q'_\beta \\ u'_\beta \end{pmatrix} = \frac{3}{16\pi}\sigma_T n'_e \int d\Omega_s I'_{in}(1 - \cos\psi'^2) \begin{pmatrix} \cos 2\chi \\ \sin 2\chi \end{pmatrix}, \tag{11}$$

where $\cos\psi' = \hat{n}' \cdot \hat{k}'_i$. If we now measure the Stokes angle with respect to the fixed vector $\hat{b} = \hat{n} \times \hat{z}/|\hat{n} \times \hat{z}|$, then the Stokes parameters are rotated by an angle -2η, where $\cos\eta = \hat{b} \cdot \hat{e}$, viz.,

$$\begin{pmatrix} q'_\beta \\ u'_\beta \end{pmatrix} \rightarrow \begin{pmatrix} q'_\beta \cos 2\eta - u'_\beta \sin 2\eta \\ q'_\beta \sin 2\eta + u'_\beta \cos 2\eta \end{pmatrix}. \tag{12}$$

Transforming to the Lab frame and averaging over directions of emitting fluid elements, we finally obtain

$$I = \frac{3}{16\pi}\int \frac{\tau}{\Gamma}\int j'_\beta \delta_n^k d\phi_\beta d\theta_\beta, \tag{13}$$

and

$$\begin{pmatrix} Q \\ U \end{pmatrix} = \frac{3}{16\pi}\int \frac{\tau}{\Gamma}\int \begin{pmatrix} q'_\beta \cos 2\eta - u'_\beta \sin 2\eta \\ q'_\beta \sin 2\eta + u'_\beta \cos 2\eta \end{pmatrix} \delta_n^k d\phi_\beta d\theta_\beta, \tag{14}$$

where $\tau = \sigma_T n_e l$ is the optical depth along the sight line, and $\delta_n = [\Gamma(1 - \beta\cos\theta_{n\beta})]^{-1}$ is the corresponding Doppler factor. The factor $1/\Gamma$ is introduced because of the transformation of the electron density from the rest frame of the fluid element to the Lab frame. Here we allow for a spread in the opening angle of the conical wall. The dependence of n_e and Γ on the angle θ_β should be specified in general. Below we examine two cases: a thin cone, defined by $n_e(\theta_\beta) \propto \delta(\theta_\beta - \theta_0)$, and a cone with a constant density in the region $\theta_0 - \Delta\theta \leq \theta_\beta \leq \theta_0 + \Delta\theta$ and zero outside this range. The index k depends, in general, on the spectrum of incident radiation, as well as on the kinematics of the emission region, and is expected to lie in the range from 2.5 to 3.5. The dependence of the polarization on k is explored below. Finally, the polarization degree is given by $P = (Q^2 + U^2)^{1/2}/I$. We note that for an axially symmetric distribution of the scattering material, the Stokes parameter U should vanish (Begelman & Sikora, 1987). As a check, we numerically computed U in each run and verified that, within the accuracy of our computation, it is zero.

We also calculate below the probability for observing a source with a polarization $P > \pi$, given explicitly by,

$$x(P > \pi) = \frac{1}{A}\int_{P(\mu)>\pi} V_{max}d\Omega = \frac{2\pi}{A}\int_{P(\mu)>\pi} I^{3/2}d\mu, \tag{15}$$

where the integration is carried over all solid angles for which the polarization fraction P exceeds the value π, and $A = \int_{P(\mu)\geq 0} V_{max}d\Omega$ is a normalization constant.

3. RESULTS

Eqs. (10) through (14) have been integrated numerically to yield the intensity and polarization of the radiation scattered off a section of the wall that moves with a given velocity. In cases corresponding to Compton sailing material, the velocity of the scattering matter was first calculated using eqs. (9) and (8). As a check on our code, we computed the scattered intensity for a point radiation source located on the symmetry axis ($a_1 = a_2 = 0$), and compared the results with the analytic approximation derived by E03. An example is shown in Fig. 3 for $z = 100$, $k = 3$, and $\theta_0 = 0.1$. The corresponding Lorentz factor of the Compton sailing fluid is $\Gamma = 101$. The numerical result is given by the dashed line and the analytic one by the solid line. We also plotted the polarization fraction P (dotted line). As seen, the agreement is good. The slight asymmetry of the dashed curve around the direction of fluid motion, $\Delta = 0$, is due to second order effects associated with the curvature of the wall which are not accounted for by the analysis of E03. Note also that the viewing angle along which the intensity peaks is slightly shifted from the direction $\Delta = 0$, and in particular does not coincide with the direction of maximum polarization. This is due to the angular dependence of the Thomson cross section. This is the reason for the relatively rapid decline of the $x(P > \pi)$ curve. As a second test case, we calculated the polarization for a radiating ring of radii $a_1 \to a_2 = 1$, with a highly beamed emission ($\theta_\gamma << 1$). This case corresponds to the head on approximation considered in Eichler and Levinson (2003). The Lorentz factor of the moving wall in this case is arbitrarily chosen (not the Compton sailing value, of course). The resultant polarization curves are displayed in Fig. 4. We find perfect agreement as $\theta_\gamma \to 0$.

The dependence of the polarization produced by a Compton sailing sheath on the various parameters is examined in Figs. 5 - 7. The upper panel in each figure exhibits the polarization fraction P versus the line of sight angle θ_n, and the lower panel the corresponding Euclidean probabilities $x(P > \pi)$, given by eq. (15), against π.

Note that in the limit that sources are so bright that they can be seen anywhere in the universe at most viewing angles, then the probability of a given polarization is indicated by $\Delta\theta$, i.e. the x axis in the upper panels of figures 5-7, except for effects from cylindrical geometry, which are small when $\theta_o\Gamma \gg 1$ and $\theta_o/\Delta\theta \gg 1$. In the opposite limit, probably not the most relevant for long, hard bursts, we assume Euclidean geometry with $V/V_{max} = .5$. The probabilities for observing polarization π almost certainly lies between these two limits.

Fig. 5 shows the dependence of the polarization curves on the opening angle of the flow, $\theta_0 = \hat{\beta} \cdot \hat{z}$. In this example $a_2 = d = 1$, that is, the radiating ring extends from the wall, and $a_1 = 0.9$, as indicated. The ring is assumed to radiate isotropically in this example (more precisely, $\theta_\gamma > 2\theta_0$ is assumed). As seen, the polarization approaches zero on the axis ($\theta_n = 0$), as required by the axial symmetry. The Lorentz factor of the Compton sailing fluid obtained in this run is $\Gamma \simeq 56$ for $\theta_0 = 0$ and , $\Gamma \simeq 57$ for $\theta_0 = 0.1$. The reason that Γ increases slightly with increasing θ_n, is that the angle between the directions of incident photons and $\hat{\beta}$ slightly decreases on the average, but since the ring radiates isotropically and the distance z from the ring to the scattering material is rather large, the effect is small. The polarization peaks at $\theta_n = \theta_0$ (but is not 100% owing to the contribution from elements moving at different ϕ_β), as long as θ_0 is not too small. Quite generally we find that the maximum polarization is suppressed for sufficiently small θ_0, as seen in Fig. 5, by virtue of the axial symmetry. The kinks in the polarizations curves correspond to a 90° change in the polarization vector.

The dependence of the polarization on the index k is displayed in Fig. 6. The Lorentz factor obtained for all cases shown in this example is 57. As seen, the P curves depend weakly on k, and mainly in the side lobes, owing to the large beaming factor of the scattered emission. The primary reason is that the main bump of the polarization curves in all cases lies in the range $\Gamma\Delta << 1$. For much smaller Lorentz factors we find somewhat stronger dependence on k. The intensity is more sensitive to k, and this is reflected in the V_{max} curves, as seen.

Fig. 7 exhibits the dependence of the polarization on the geometry of the incident radiation source. Three cases are examined: a point source ($a_1 = a_2 = 0$), a disk extending from the wall ($a_1 = 0$, $a_2 = 1$), and an infinitely thin ring ($a_1 = a_2 = 1$). As seen, a point source gives rise to a nearly maximum polarization in the direction $\theta_n = \theta_0$, as expected in the limit of large beaming. This is due to the fact that all incident rays are perpendicular to the direction of motion in the comoving frame. The peak of the polarization curve is smaller in the case of an extended source by virtue of the finite range of incidence angles, but is still rather high for sufficiently large Lorentz factors ($\Gamma = 64$ in the case of the disk and 56 for the thin ring).

In Fig. 8 we explore how the polarization depends on the Lorentz factor of the Compton sailing matter. All three cases shown were calculated using a point radiation source ($a_1 = a_2 = 0$). The source is located at a different distance from the scattering material in each case. The Lorentz factors of the sailing material, roughly equal $\Gamma = (z^2 + d^2)^{1/2}/d$ are indicated. As expected, the maximum polarization is reduced for small Lorentz factors, owing to the larger contribution from fluid elements located at larger angular separation with respect to the sight line. We found, however, that the cumulative probability curves converge to the solid line for $\Gamma > 25$, as can be inferred from the figure.

Fig. 9 examines the effect of Compton sailing. Here we compare the cumulative V_{max} curve obtained in the Compton sailing case (indicated as Γ_c in the figure) with cases obtained when the Lorentz factor deviates from this value. We also plotted for comparison the result obtained in the head on approximation in the limit $\Gamma\theta_0 \to 0$ (Eichler and Levinson 2003). It is seen that Compton sailing greatly increases the likelihood of strong polarization.

The results described above correspond to an infinitely thin cone with an opening angle θ_0. The effect of a spread in the opening angle of the cone of optically thin scattering material is examined in Fig. 10. In this example the velocity vectors are assumed to lie in the range between $\theta_0 - \Delta\theta$ and $\theta_0 + \Delta\theta$. All fluid elements are assumed to move with their Compton sailing Lorentz factor. As seen, the polarization is lowered when $\Delta\theta$ is much larger than $1/\Gamma$, but, in the absence of any cylindrical symmetry around the line of sight, does not plummet to zero in this limit.

Finally, the effect of photon diffusion in cases of a large optical depth is depicted in Fig. 11. Solving the radiative transfer in a medium with a modest optical depth is a formidable task, and is beyond the scope of this paper. Here we consider diffuse reflection from a plane parallel, semi-infinite slab. We suppose that in the comoving frame the radiation incident normal to the wall, and use the results derived in Chandrashekar (1960) for the polarized intensity reflected off the wall. We then transform the intensities back to the Lab frame in order to compute the probability $x(P > \pi)$. The upper panel exhibits the polarization curve and the (normalized) Euclidean V_{max} curve, and the lower panel the cumulative probability as usual. The direction of maximum polarization is along the wall of course, with peak polarization of 0.47. The total intensity of the reflected radiation increases with increasing angle from the wall, and is maximum at an angle of $1/\Gamma$, as measured in the Lab frame (about a factor of 2 larger than along the wall). This is reflected in the shape of the V_{max} curve.

4. CONCLUSIONS

We have shown, under less simplified assumptions than made in Eichler (2003), that when matter is Compton dragged into a "sailing" equilibrium by photons, the polarization can be quite high for singly scattered photons. The direction of maximum polarization coincides with the maximum intensity of the polarized component. Finite source size is found to not qualitatively alter this conclusion. Finite source angular width $\delta\theta$, which can nearly eliminate net polarization in most models, is found in the present model to reduce it only somewhat, and to leave about 40 percent polarization for most relevant viewing angles.

In the picture presented here, singly scattered photons may in principle compete with unscattered ones, because the photon energy as seen in the lab frame is not dramatically altered. [This is in contrast to the scenario of Shaviv and Dar, 1995, Lazzati et al. 2000, where the photon energy is dramatically raised by the scattering, so that virtually all the gamma rays are attributed to such scattering.] However, the scattered and unscattered photons do not necessarily arrive at the same time, are not concentrated in the same directions, and do not necessarily

have exactly the same spectrum. [In some cases, the line of sight does not necessarily admit unscattered photons, e.g. as was argued (Nakamura 1998, Eichler and Levinson 1999) for the case of GRB980425, however, this GRB may be exceptional.] It is thus important that future GRB polarization experiments be sensitive to the polarization as a function of time and energy range.

If the photons are scattered (undergoing "diffuse reflection" in the terminology of Chandrasekhar, 1960) off an optically thick sheath, then the maximum polarization corresponds to 47 percent along the direction of maximum intensity of the polarized component. Typically, polarizations of 30 to 47 percent are expected in this situation among the scattered photons. Consistently observed values in this range of polarizations, with a sharp cutoff at 47 percent, might thus be a signature of diffuse reflection.

The situation in which the optical depth of the scatterers is slightly greater than unity remains to be studied in detail. We believe that the results will be not too much different from the case of single scattering, because the path of maximal polarization corresponds to minimum optical depth in a relativistically expanding flow. In any case, they should lie between the two extremes considered in this paper. It might be claimed that an optical depth of order unity is "fine tuned". However, in the present picture, the sheath tapers to infinity, so most of its area is in fact comprised of material with an optical depth of order unity. The path of least optical depth is along the direction of motion, because then the relative velocity between the photon and the material, as seen by the lab frame is the smallest (Levinson and Eichler, 2003).

If future polarization studies eventually show some indication of scattering of GRB photons, correlation between maximum polarization and maximum intensity might provide clues as to whether energy is indeed flowing from the scattering material to the photons or whether most of the scattering occurs after Compton equilibrium has been reached, which would suggest that matter is being dragged by the photons rather than upscattering them.

REFERENCES

J-L. Atteia, G.R. Ricker, D.Q. Lamb, T. Sakamoto, C. Graziani, T. Donaghy, C. Barraud, & the HETE-2 Science Team, 2003, SF2A confE, 167
Begelman, M.C., & Sikora, M., 1987, ApJ, 322, 650
Chandrashekar, S. 1960, Radiative Transfer, (Dover)
Coburn, W. & Boggs, S.E., 2003, Nature, 423, 415
Dado, S., Dar, A. & De Rujula, A., 2003, A & A, 388, 1079
Dar, A. & Shaviv, N., 1995, Phys. Rev. Lett., 75, 3052
Eichler, D., 1994, ApJ Supp., 90, 877
Eichler, D., 2003, astro-ph/0309092
Eichler, D. & Levinson, A., 1999, ApJ, 521, L117
Eichler, D. & Levinson, A., 2000, ApJ, 529, 146
Eichler, D. & Levinson, A., 2003, ApJ, 596L, 147
Hajdas, W., Wigger, C., Guedel, M., Mchedlishvili, A. & Smith, A. D., 2003, Proc. of "Particle Acceleration in Astrophysical Objects", Cracow

Lazzati, D. Ghisselini, G. Celotti A. & Rees, M.J., 2000, ApJ, 529, L17
Levinson, A. & Eichler, D., 1993, ApJ, 418, 386
Levinson, A. & Eichler, D., 2000, Phys. Rev. Lett., 85, 236
Levinson, A. & Eichler, D., 2003, ApJ, 594, L19
Lyutikov, M., Parlev, V.I. & Blandford, R., 2003, astro-ph 0305430
Nakamura, T., 1998, Prog. Theor. Phys., 100, 921
Phinney, E., 1982, MNRAS, 198, 1109
Preece, R.D. et al., 2002, ApJ, 581, 1248
Shaviv, N. & Dar, A., 1995, MNRAS, 277, 287
Shaviv, N. & Dar, A., 1995, ApJ, 447, 863
van Putten, M. & Levinson, A., 2002, Sci, 295, 1874
van Putten, M. & Levinson, A., 2003, ApJ, 584, 937
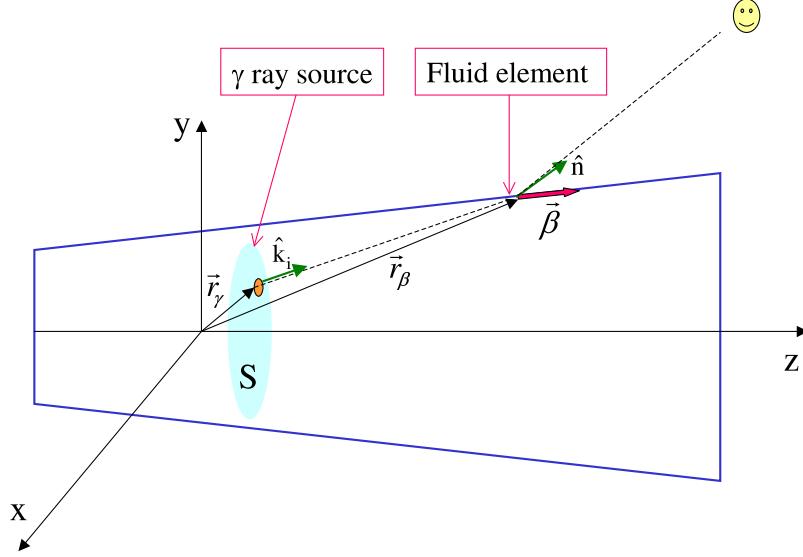
Fig. 1.— Schematic illustration of scattering by a relativistic sheath. Gamma rays are emitted from a surface marked as S in the figure, and scatter off matter that ensheath the ultrarelativistic, optically thin core. The symmetry axis of the system is taken to be in the z-direction. The position of a scattering center on the wall, moving with a velocity $\vec{\beta}$, is defined by the vector $\vec{r}_\beta$. The position vector of a point on the gamma-ray emitting surface is labeled by $\vec{r}_\gamma$. The sight line direction is denoted by $\hat{n}$.
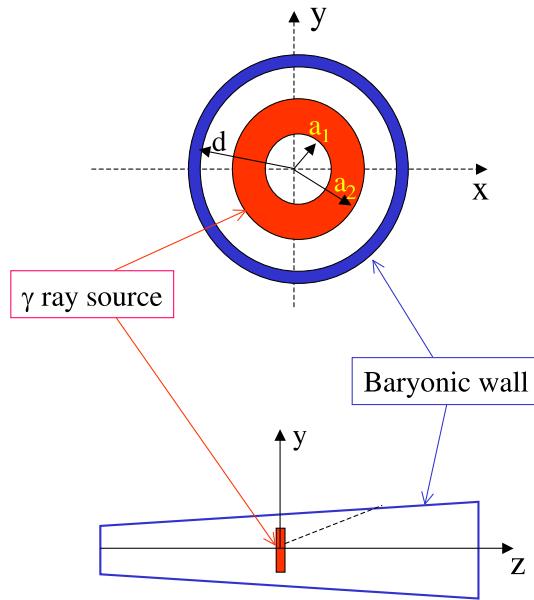
FIG. 2.— A sketch of the radiation source geometry adopted for the calculations is shown. The emitting surface has a geometry of a ring with inner and outer radii denoted by a_1 and a_2, respectively. The ring lies in the (x, y) plane at $z = 0$ and is centered around the symmetry axis of the system. The radius of the wall containing the scattering material at $z = 0$ is denoted by d.
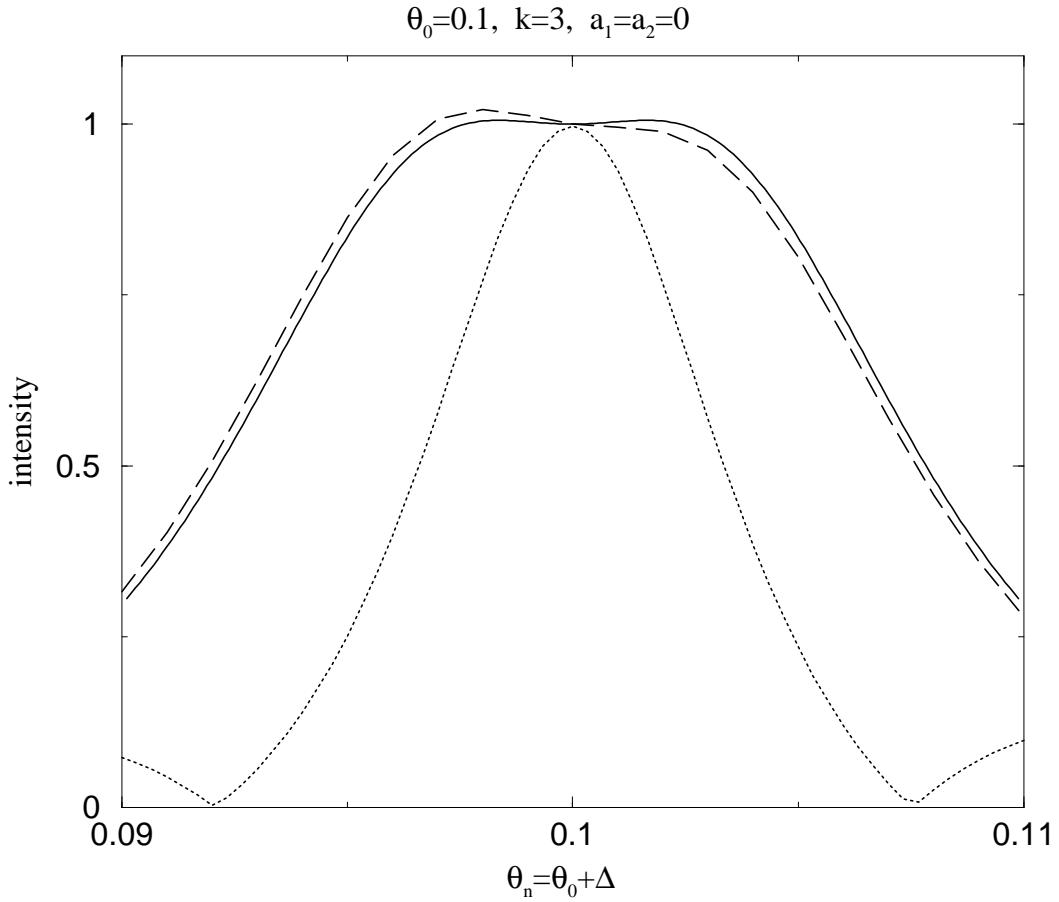
FIG. 3.— Scattered intensity (dashed lines) and polarization degree (dotted line), calculated using a point radiation source located on the symmetry axis, are plotted as a function of viewing angle θ_n. A plot of the intensity calculated using the analytic approximation derived in Eichler (2003) is shown for a comparison (solid line). The parameters θ_0 and k are defined in the text.
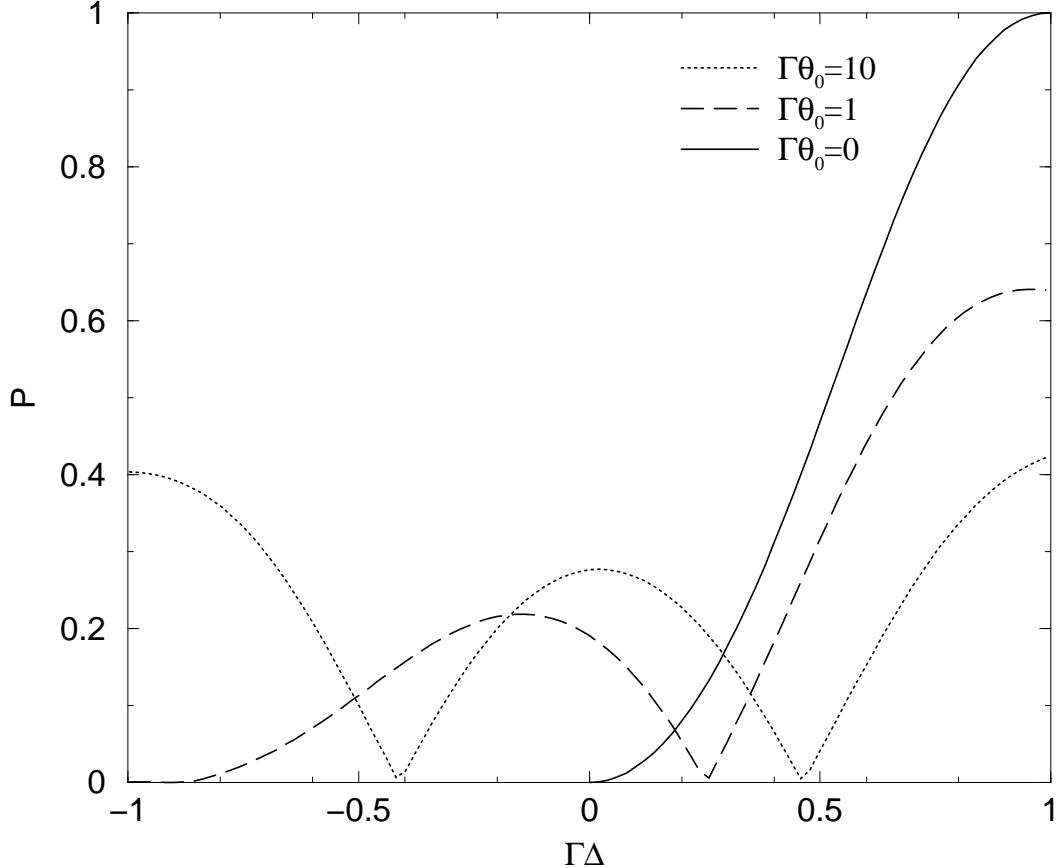
FIG. 4.— The polarization degree as a function of $\Gamma(\sin\theta_0 - \sin\theta)$, calculated numerically using a radiating ring with $a_1 = a_2 = 1$ and highly beamed emission for different values of $\Gamma\theta_0$, is shown for the purpose of comparison with the results obtained in the head on approximation by Eichler and Levinson (2003).
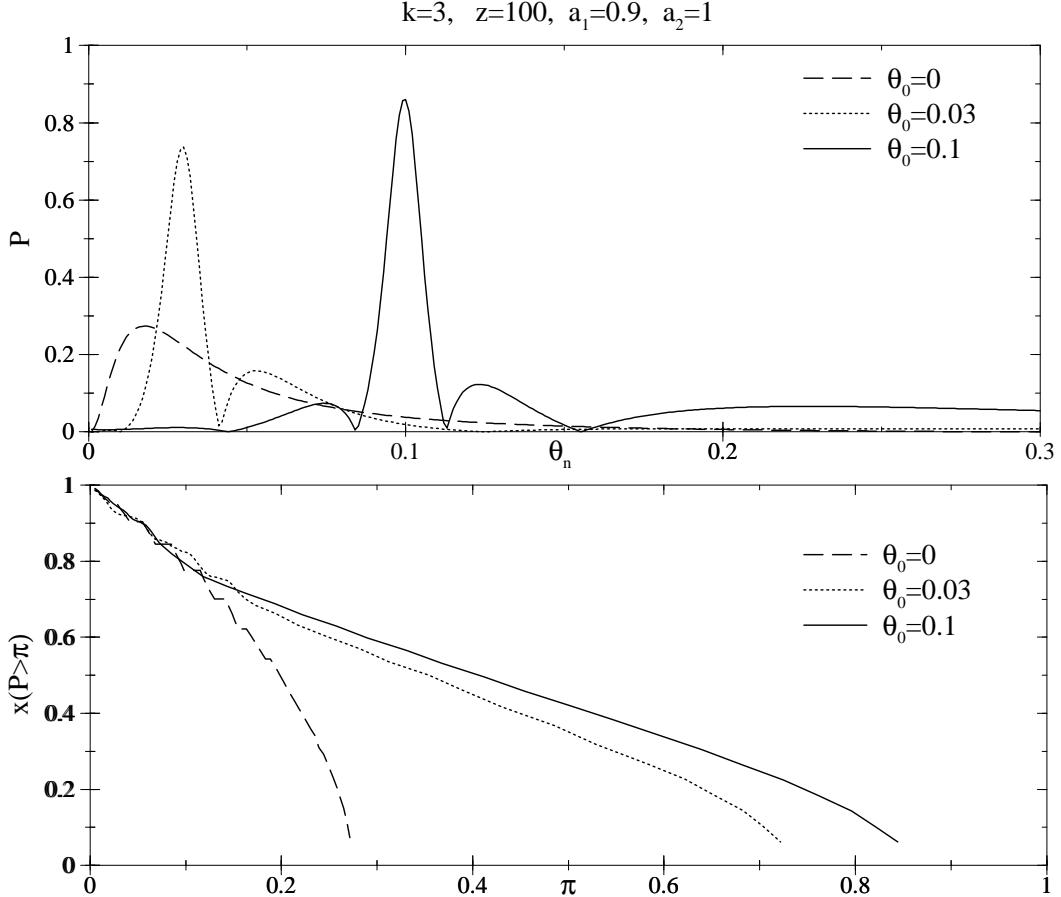
FIG. 5.— The upper panel exhibits polarization curves for different values of the opening angle θ_0. The polarization in the inner bump is parallel to the wall, and changes by 90° across the kinks. The bottom panel displays the corresponding probability for observing a source with polarization higher than π, as given by eq. (15) in the text.
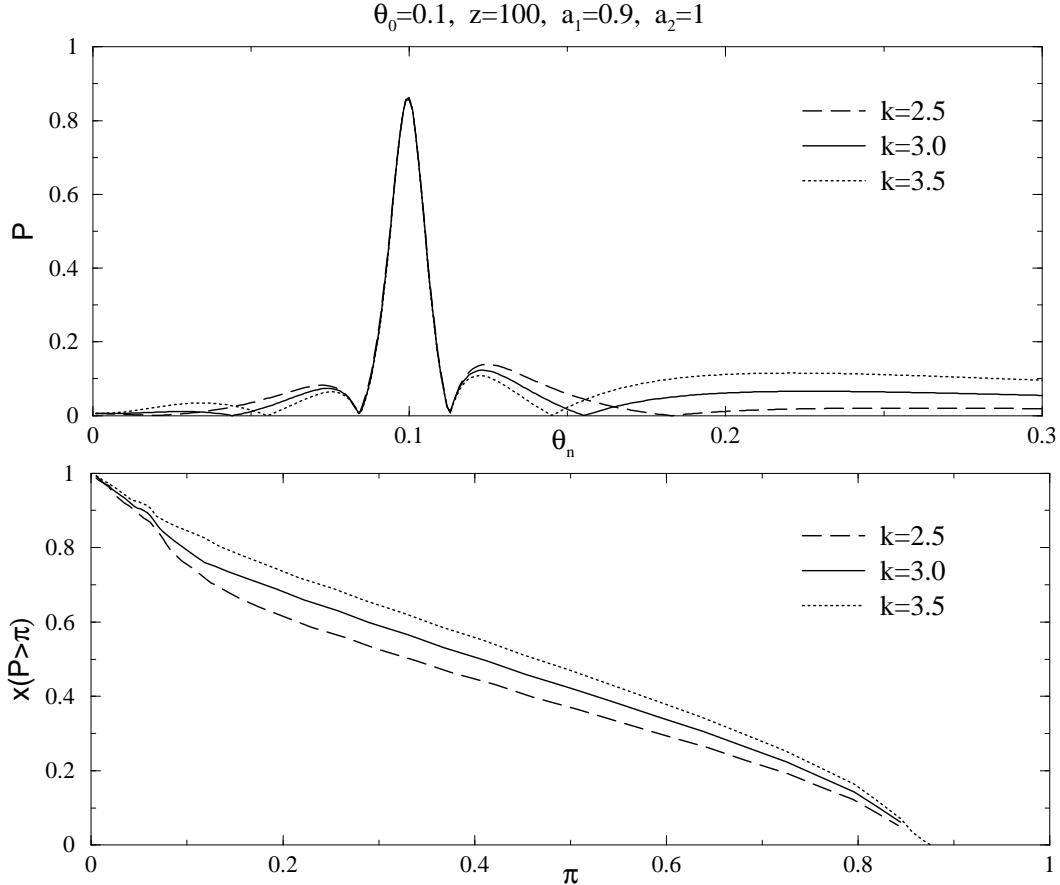
FIG. 6.— Same as Fig. 5, but for different values of the index k.

$\theta_0=0.1, \ z=100, \ k=3$
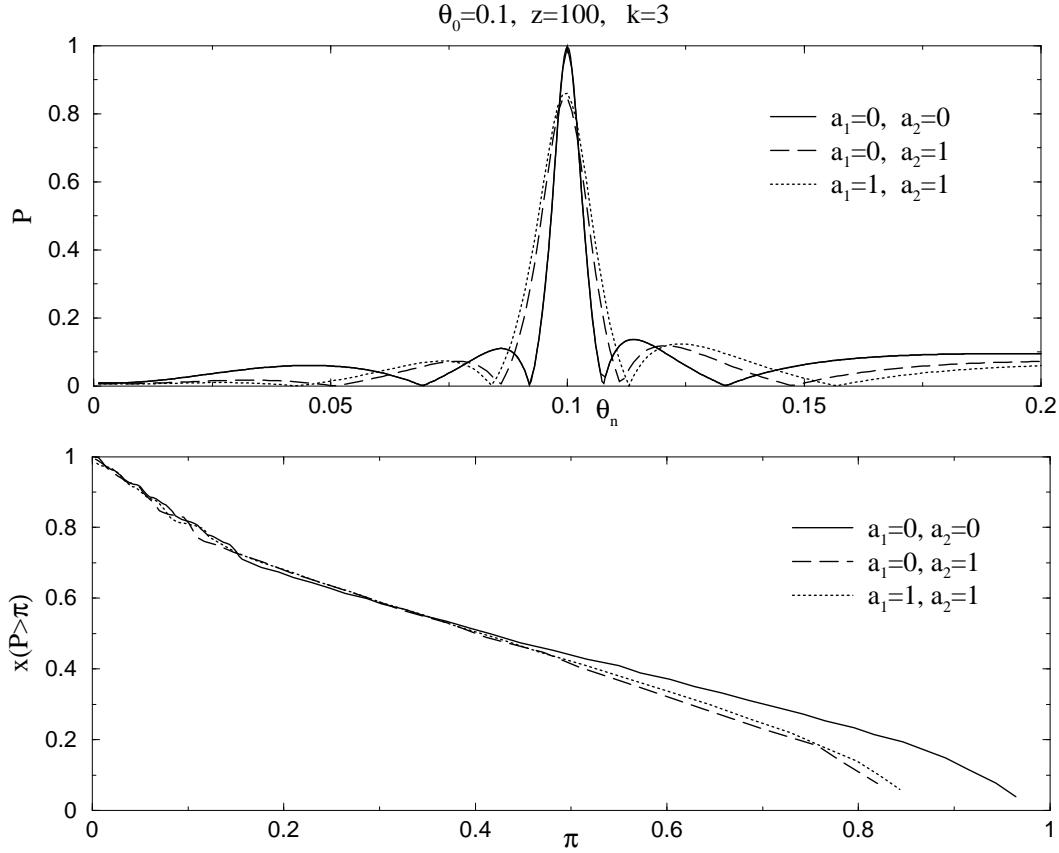
Fig. 7.— Same as Fig. 5, but for different ring parameters
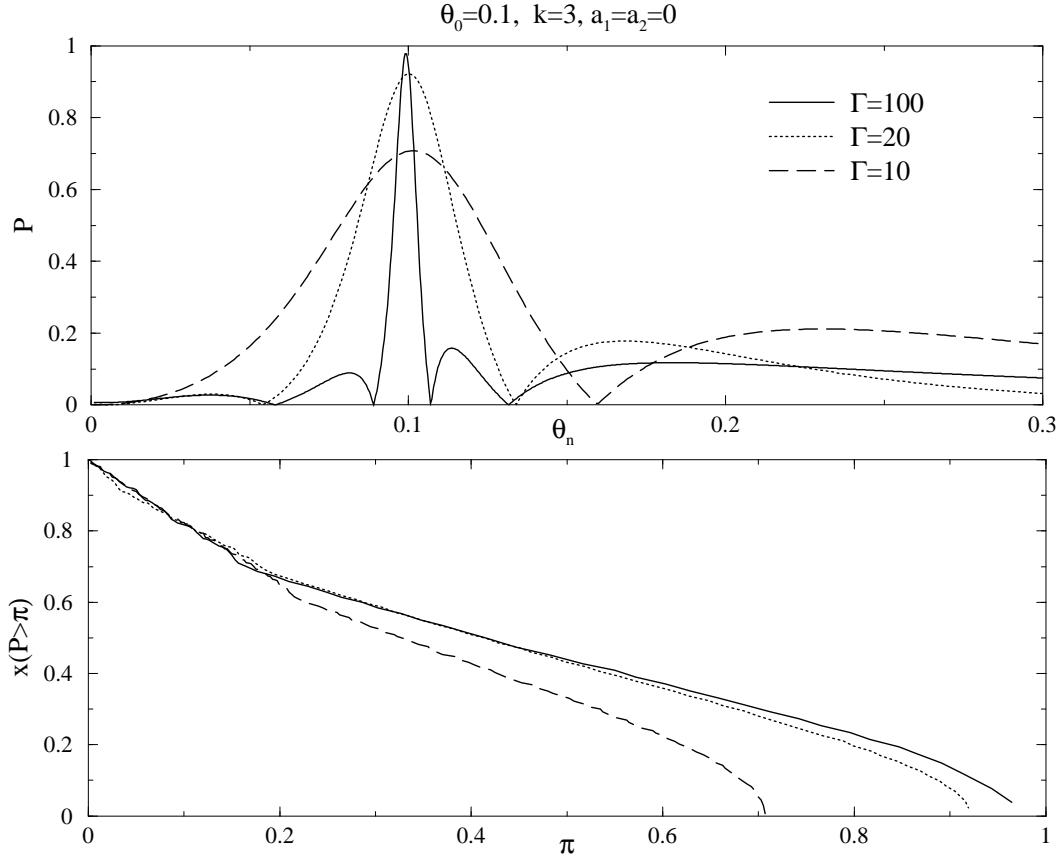
FIG. 8.— Dependence of polarization on the Lorentz factor of the Compton sailing matter. All cases shown were calculated using a point radiation source.
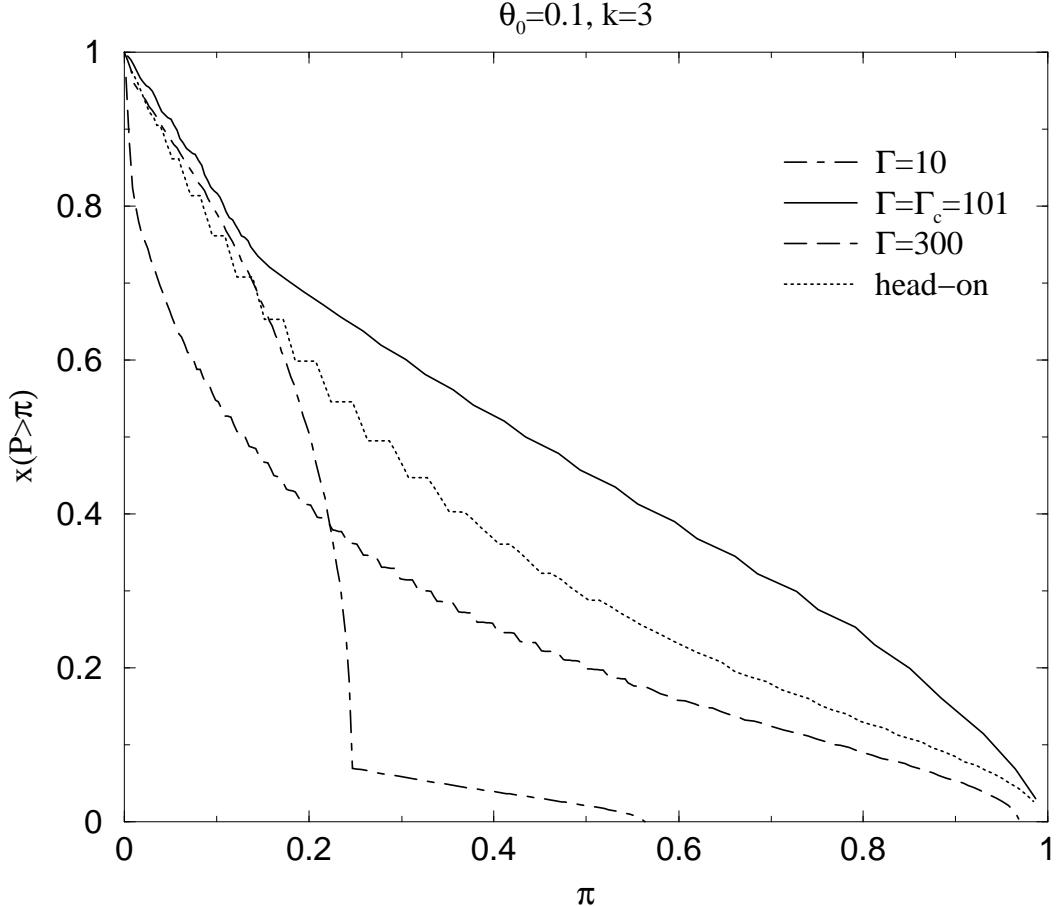
FIG. 9.— Comparison of the cumulative probability curves obtained for a Compton sailing wall (indicated by Γ_c), with those obtained in cases where the Lorentz factor of the scattering material deviates from the Compton sailing value (see text for further discussion).
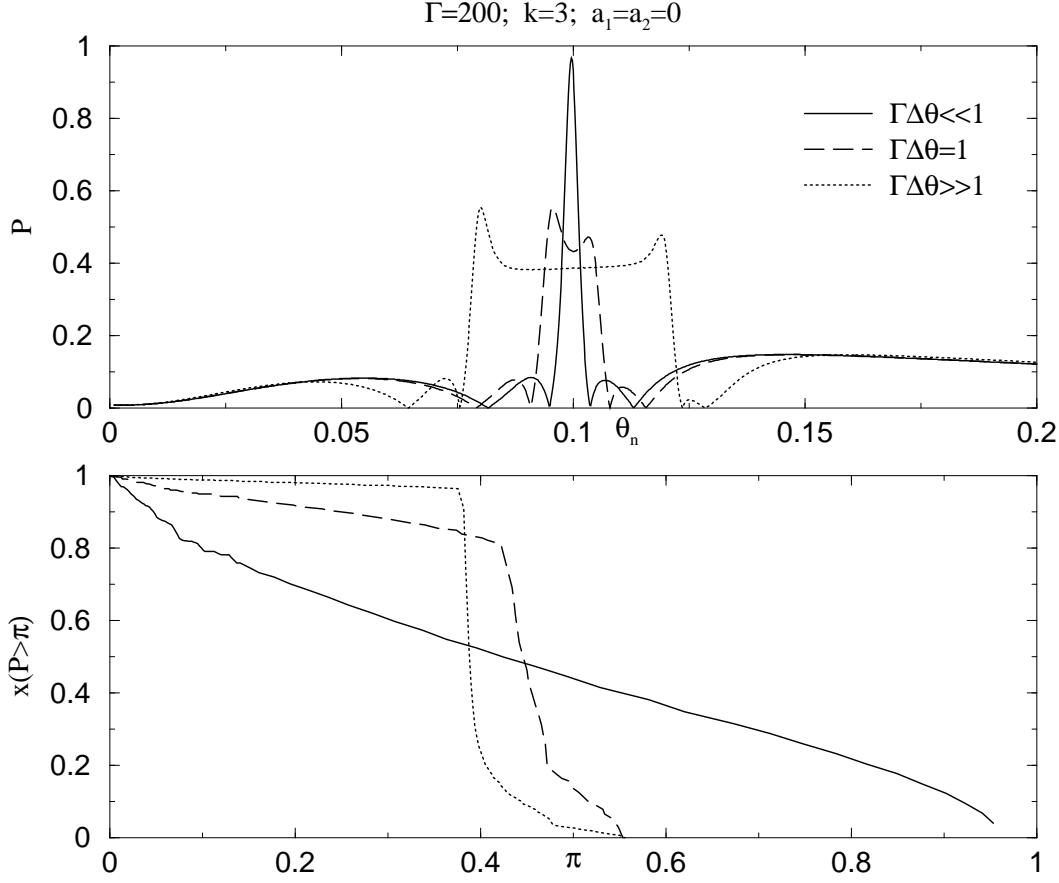
FIG. 10.— The polarization produced by scattering off a matter moving on conical shells encompassing a range of opening angles between $\theta_0 - \Delta\theta$ and $\theta_0 + \Delta\theta$. Each sub-shell is coasting with a Lorentz factor corresponding to the Compton sailing value. The Loerntz factor of the central sub-shell is indicated..

Γ=100
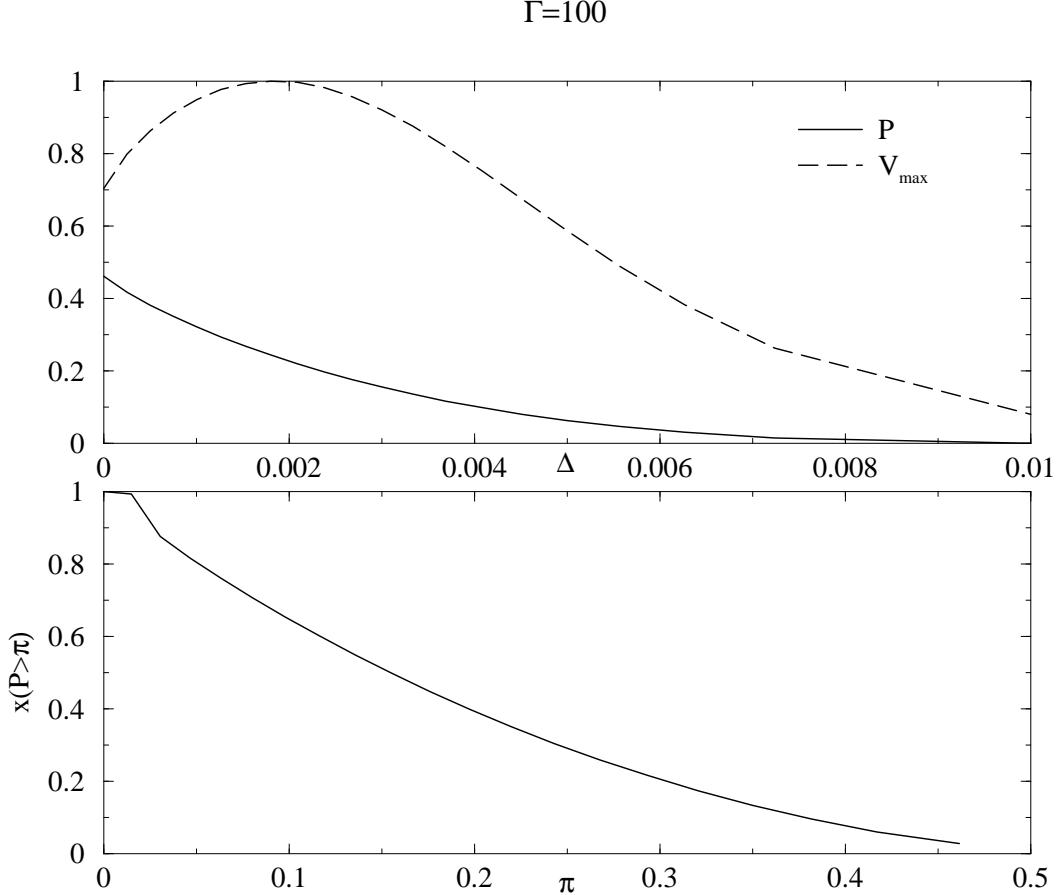
FIG. 11.— Effect of multiple scattering inside the wall on the polarization of emergent radiation. Shown are the polarization of a radiation reflected off a semi-infinite, plane-parallel slab, as a function of the angle Δ from the wall (upper panel), and the cumulative probability (lower panel) . The direction of the incident beam is taken to be normal to wall in the wall's rest frame.